Quantum-Defect Theory of Double-Minimum States in H_2

S. Ross and Ch. Jungen
Laboratoire de Photophysique Moléculaire du Centre National de la Recherche Scientifique, Université Paris-Sud, 91405 Orsay, France

(Received 23 July 1987)

Scattering theory is used to calculate the vibronic energy levels of the interacting double-minimum states in H_2. The calculation is based on the accurate *ab initio* fixed-nuclei energies of Wolniewicz and Dressler. From these a nondiagonal reaction matrix is extracted whose elements are nuclear-coordinate dependent and involve singly and doubly excited channels. The treatment bypasses the state-by-state evaluation of vibronic coupling, and yields in principle the entire vibronic Rydberg spectrum associated with the $H_2{}^+$ $1\sigma_g$ and $1\sigma_u$ cores. The first forty experimental levels are reproduced quite accurately.

PACS numbers: 31.60.+b, 33.10.Cs, 34.10.+x, 34.80.Kw

An ever recurring problem in molecular physics concerns the breakdown of the Born-Oppenheimer separation[1] of nuclear and electronic motion. While this breakdown is usually only local in the lower electronic states of a molecule, it occurs systematically in highly excited states, and is complete in the electronic continuum. A classic example of strongly correlated nuclear and electronic motion occurring at relatively low energy is furnished by the manifold of totally symmetric ($^1\Sigma_g^+$) electronic states of diatomic hydrogen.[2-4] Figure 1 displays the five lowest excited $^1\Sigma_g^+$ electronic states of H_2 plotted as functions of the internuclear distance. Successive curves exhibit quite different shapes, and close approaches occur for a number of R values. Previous calculations of the strongly perturbed vibrational-electronic ("vibronic") levels associated with these potential wells have proceeded on a state-by-state basis. Thereby the vibronic coupling function between each pair of electronic energy curves is evaluated separately from accurate two-electron wave functions over the range of relevant R values, and a system of coupled equations is then solved.[5] Extension of this approach beyond the first few states is not feasible, and the precise connection between the vibronic interactions among bound levels and the related inelastic continuum processes at higher energies is difficult to establish. Such processes include collisions between two open-shell H atoms (leading, e.g., to associative ionization), or collisions between an electron and a vibrating molecular $H_2{}^+$ ion (leading, e.g., to dissociative recombination), and also molecular preionization and predissociation.

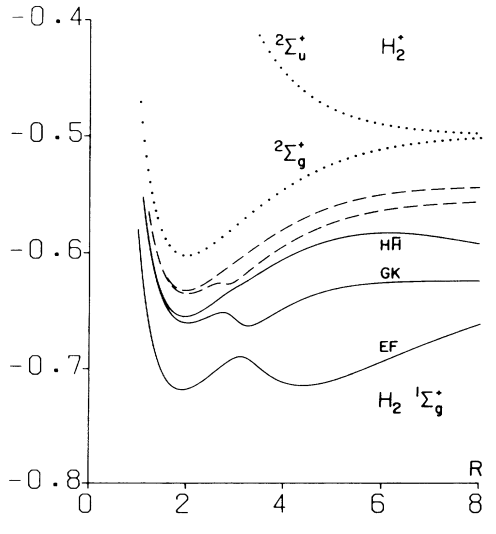

FIG. 1. Potential energy curves of $^1\Sigma_g^+$ symmetry for H_2 (atomic units). The first two curves of $H_2{}^+$ are also shown (dotted lines).

In this Letter we treat the vibronic states associated with the potential wells depicted in Fig. 1 *globally*, as resulting from a vibrationally and electronically inelastic "scattering" process taking place at negative energy. The multichannel quantum-defect method (MQDT)[6] is, for our purposes, a convenient form of scattering theory extended to the description of bound states in neutral systems. Developed initially for the description of atomic Rydberg series,[6] MQDT has in recent years been applied to a broad range of problems in atomic and molecular physics.[7,8] Its power derives from the fact that continua and bound levels are treated on the same footing. Indeed, each family of bound levels is regarded as just the "closed" portion of a decay channel. The method is therefore particularly suited for the description of *resonances*. The novel feature of our present application is the demonstration that the three lowest fixed-nuclei curves of Fig. 1 implicitly contain *all* information that is required to account for the *full* dynamics of electronic and nuclear motion in these states. The explicit calculation of vibronic coupling matrix elements is entirely bypassed in our approach. Extension of the treatment to the so far only poorly understood higher states near the ionization threshold[9] and to the continuum above it is, in principle, straightforward, and should be possible on the basis of the molecular parameters derived here. On the other hand, the extension to molecular dissociation processes will require an additional development.

Electronically highly excited states of neutral systems fall into Rydberg series such that their energies can be presented by a Rydberg-type equation

$$\tan\pi\nu(\epsilon)+\tan\pi\mu=0, \quad (1a)$$

$$\nu(\epsilon)=(-2\epsilon)^{-1/2}, \quad (1b)$$

where ϵ is the binding of the excited (Rydberg) electron in atomic units. Equation (1a) is the quantum condition for obtaining a bound level, namely, that the accumulated radial phase $\pi\nu(\epsilon)$ of the Rydberg electron at infinity be an integer.[10] ν is the effective principal quantum number familiar from atomic physics. μ is the familiar "quantum defect"; $\pi\mu$ is the additional radial phase due to the non-Coulombic short-range interactions. When the ion core has no internal structure, such as in the case of a hard sphere,[11] the quantum defect is a virtually energy-independent quantity characterizing the whole infinite series represented by Eqs. (1).

An intriguing feature with regard to Fig. 1 is that both in the united-atom limit $[R=0, \mathrm{He}(1s,nl)]$ and in the separated-atom limit $[R\to\infty, \mathrm{H}(1s)+\mathrm{H}(nl)]$ the series of ${}^1\Sigma_g^+$ states can be represented by Eqs. (1) with nearly $(R=0)$ or exactly $(R\to\infty)$ energy-independent quantum defects. For intermediate R values, the curves shown in Fig. 1 can still be formally represented by Eqs. (1), but the quantum defect now has a complicated dependence $\mu(\epsilon,R)$ on the energy as well as on the internuclear distance. Although this is not directly obvious from Fig. 1, this double parametric dependence of the electronic phase shift is entirely analogous to the dependence encountered in resonant electron-molecule scattering problems.[12]

We proceed from here by noting that in the present problem the resonant behavior of the quantum defect reflects the interactions between three Rydberg series or electronic channels. When the Rydberg electron is far removed from the $\mathrm{H_2}^+$ ion these channels can be identified as $(\mathrm{H_2}^+,e^-)$: $(1\sigma_g,s\sigma_g)$, $(1\sigma_g,d\sigma_g)$, and $(1\sigma_u,p\sigma_u)$. $1\sigma_g$ and $1\sigma_u$ are the two lowest electronic states of $\mathrm{H_2}^+$, also represented in Fig. 1. We use the l value of the outer electron as a convenient short-hand notation and label the three relevant electronic channels as s, d, and p, respectively.

We know from the work of Seaton[6] that the resonant behavior of the quantum defect in a multichannel problem can be removed or "smoothened," by the use of a generalized multichannel version of Eqs. (1) which explicitly allows for inelastic short-range processes, such as the excitation $\mathrm{H_2}^+$ $1\sigma_g\to 1\sigma_u$ in our example. Specifically, the quantum defect in Eq. (1a) is now converted into a nondiagonal quantum-defect matrix $\mu_{ll'}$. The corresponding short-range reaction matrix is $K_{ll'}=\tan\pi\mu_{ll'}$. Since outside the ion core the motion of the outer electron is expected to remain independent in different channels, the term representing the asymptotic motion in Eqs. (1) generalizes into $\tan\pi\nu_l(\epsilon_l)\delta_{ll'}$. [To be precise, we use a variant of Eq. (1a) corresponding to a different normalization of the radial Coulomb functions than implied by Eqs. (1) and where the μ quantum defect is replaced by the so-called "η defect."[6]]

The next stage involves the determination of the nondiagonal quantum-defect matrix for the excited ${}^1\Sigma_g^+$ states of $\mathrm{H_2}$. Our approach has been to use to the best advantage the extremely precise *ab initio* Born-Oppenheimer ("fixed nuclei") potential functions calculated[13] for the *EF*, *GK*, and $H\bar{H}$ states. These potential functions are shown by the lowest three curves (solid) in Fig. 1. It is, however, not possible to perform a direct least-squares fitting, for each internuclear separation, of the elements of the quantum-defect matrix to the *ab initio* potentials. This is because the μ matrix contains *six* independent elements for each value of R, whereas only three *ab initio* energies are available at each R. It was therefore necessary to include other information in the procedure for determining the μ matrix. In particular, for large internuclear spacings, μ must approach a form corresponding to two separated hydrogen atoms, and in the limit $R\to 0$ it must correspond to the helium atom. We shall take the μ matrix to be diagonal in both limits. Further, the elements of μ are expected to be smooth functions of R. This smoothness was imposed on the quantum defects by only defining them on fairly widely spaced grids of internuclear bond lengths. Values between the points were obtained by spline interpolation. To simplify the problem somewhat we have neglected *direct* mixing between the s and d channels by fixing $\mu_{sd}=0$ for all R. This mixing is less important than the *s-p* and *d-p* mixing and in any case *indirect s-d* mixing, through their mutual interactions with p, is included.

Through a cyclical series of partial least-squares fittings and manual adjustments of the grid points, the final set of quantum defects shown in Fig. 2 was obtained. The solid curves correspond to the diagonal elements of the quantum-defect matrix and, thus, to the "diabatic" channels, while the dashed curves are the *s-p* and *d-p* interaction defects. These defects, through the multichannel version of Eqs. (1), reproduce the *EF*, *GK*, and $H\bar{H}$ potential curves of Ref. 13 to within 10 cm^{-1} (5×10^{-5} a.u.). On the scale of Fig. 1 this corresponds to $\frac{1}{15}$ of the line thickness. (It was found to be necessary to include a small residual energy dependence in the μ_{ss} defect.)

The quantum-defect matrix of Fig. 2, however, does not just describe the first three excited states of ${}^1\Sigma_g^+$ hydrogen, but, to the extent that its elements are independent of the energy, the entire set of excited ${}^1\Sigma_g^+$ state curves is implicitly contained therein. The broken curves of Fig. 1 represent the next two higher states as obtained from the MQDT. Note how the $5\,{}^1\Sigma_g^+$ curve has an appearance quite different from the 2, 3, and $4\,{}^1\Sigma_g^+$ curves

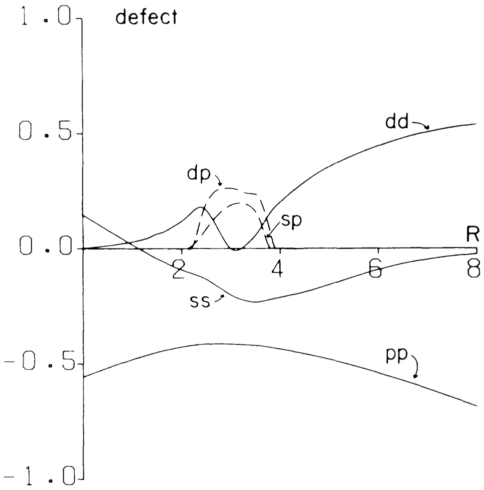

FIG. 2. Diagonal (solid lines) and off-diagonal (dashed lines) elements of the quantum-defect matrix representing the states shown in Fig. 1.

that were the sole basis for the determination of the μ matrix from which it was obtained. Indeed, the form of the $5\,^1\Sigma_g^+$ potential curve is very similar to that obtained in an approximate *ab initio* calculation (shown in Fig. 1 of Wolniewicz and Dressler[14] and labeled "$4d\sigma$" there). Since the calculation was not quite converged, the computed energies are expected to lie higher than the true energies. We have found that, indeed, the curve which we predict on the basis of the quantum-defect matrix of Fig. 2 lies consistently somewhat lower than the approximate *ab initio* curve. The deviation, however, does not exceed 0.0018 a.u., or 2.5 times the line thickness on the scale of Fig. 1.

This result is important for the following since it confirms that the quantum-defect matrix is virtually *energy independent* over the range of at least 0.1 a.u. and possibly considerably more. This *nonresonant* behavior of the short-range quantum-defect matrix (or the equivalent electronic phase shifts) implies[15] that the excited electron spends very little time in the reaction zone in excess of its motion under the influence of the long-range field alone. We may therefore assume that the nuclei are *frozen* when both electrons are in the reaction zone. This assumption has previously been used for electronically *elastic*-scattering processes (in neutral systems particularly for the *ungerade* manifold of H_2 states, see Ref. 8); it is extended here to electronically *inelastic* processes for the first time. Accordingly, a vibrational-electronic reaction matrix can be constructed with simple integrals involving vibrational wave functions of the ion core:

$$K_{lv,l'v'}=\int dR\,\chi_v^{(l)}(R)\tan\pi\mu_{ll'}(R)\chi_{v'}^{(l')}(R). \qquad (2)$$

This expression replaces the short-range term $\tan\pi\mu$ in Eqs. (1) and correspondingly, for each total energy E, the electron energy ϵ_{lv} in the long-range term relating to the channel l,v is now taken relative to the appropriate vibrational-electronic internal state of $H_2{}^+$.

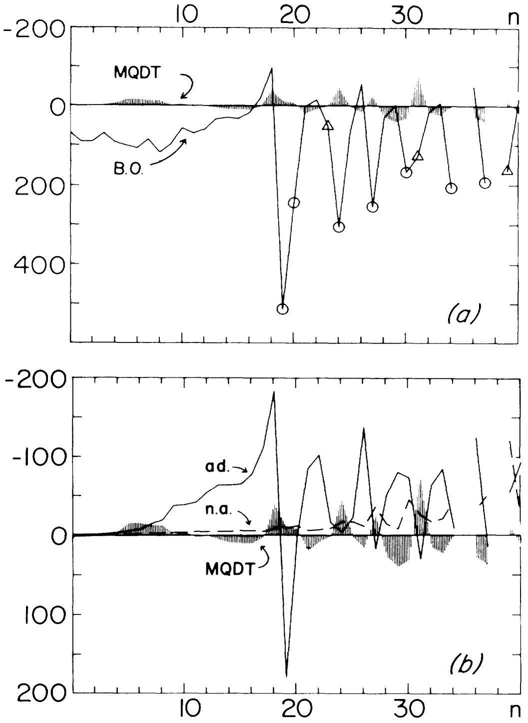

FIG. 3. Deviations (observed − calculated) for the vibronic levels associated with the states of Fig. 1 (cm^{-1}). (a) Born-Oppenheimer approximation (full line). Levels associated with the GK ($H\bar{H}$) state are marked by circles (triangles). Present calculation (vertical shading). (b) Adiabatic approximation (full line), nonadiabatic calculation (dashed line), and present calculation (vertical shading). The levels $n=35$ and 38 have not yet been observed.

The calculation of the vibronic energy levels with total angular momentum $J=0$ was carried out in two steps. First, the K matrix elements of Eq. (2) were evaluated numerically for $l=s$, d, and p and $0\le(v,v')\le 39$, 39, and 94, respectively. The vibrational wave functions were evaluated with the $1\sigma_g$ and $1\sigma_u$ fixed-nuclei potential curves for $H_2{}^+$, to which we added the appropriate rotational energies and the adiabatic corrections for electron kinetic energy associated with nuclear motion. The vibrational spectrum of the $1\sigma_u$ states is continuous. We have selected the vibrational functions which at $R_c=15$ a.u. are zero. This set is discrete and complete for $R\le R_c$, but restricts the calculation to vibronic levels with negligible amplitude for $R\ge R_c$. In the second step, the generalized Eqs. (1) were solved. Account was taken of the finite proton masses in Eq. (1b).

The results obtained to date are illustrated in Fig. 3. Here the observed − calculated energies are plotted as functions of the index n which enumerates all the $^1\Sigma_g^+$,

$J=0$ levels in energetic order. Figure 3(a) compares the agreement with experiment[3,4,16,17] obtained from the MQDT with that obtained by direct numerical integration of the vibrational wave functions on the *same* fixed-nuclei potentials as were used above to obtain the quantum-defect matrix. The improvement obtained in using the MQDT is striking. Wolniewicz and co-workers have used *ab initio* theory in successive approximations to account for the vibration-electron coupling among the levels in the first three excited ${}^1\Sigma_g^+$ states. In Fig. 3(b) the same MQDT results shown in Fig. 3(a) are compared with the agreement with experiment obtained in the latest adiabatic[13] and nonadiabatic[18] calculations. It is clear from Fig. 3(b) that the MQDT results, derived from the fixed-nuclei potential curves, represent a decisive improvement over the adiabatic calculations and that the bulk of the nonadiabatic corrections has indeed been accounted for.

One of the great advantages of the MQDT lies in its potential to explore increasingly higher energy regions where the density of electronic states grows explosively and the Born-Oppenheimer approximation becomes increasingly inappropriate as a starting point. In fact, the quantum-defect matrix already determined should implicitly contain all of the complicated vibronic coupling for *all* vibronic levels up to and beyond the ionization limit with no further information required. This extension is in progress. For example, we have calculated the $v=0$ level of the $5\,{}^1\Sigma_g^+$ state (or $4d\sigma P\,{}^1\Sigma_g^+$) for which no precise *ab initio* results exist. The converged MQDT energy for this level is 117422 cm^{-1}, in good agreement with the experimental value of 117437 cm^{-1}.[3]

This work was supported in part by the Swiss National Science Foundation while one of us (S.R.) held a guest appointment at the Swiss Federal Institute of Technology in Zürich. We thank K. Dressler (Zürich) for reading the manuscript.

---

[1] M. Born and J. R. Oppenheimer, Ann. Phys. (Leipzig) **84**, 457 (1927).

[2] G. H. Dieke, Phys. Rev. **76**, 50 (1949).

[3] H. M. Crosswhite, *The Hydrogen Molecule Wavelength Tables of Gerhard Heinrich Dieke* (Wiley-Interscience, New York, 1972).

[4] L. Wolniewicz and K. Dressler, J. Mol. Spectrosc. **67**, 416 (1977).

[5] K. Dressler, R. Gallusser, P. Quadrelli, and L. Wolniewicz, J. Mol. Spectrosc. **75**, 205 (1979).

[6] M. J. Seaton, Rep. Prog. Phys. **46**, 167 (1983).

[7] U. Fano, Phys. Rev. A **2**, 353 (1970).

[8] See the review by Chris H. Greene and Ch. Jungen, Adv. At. Mol. Phys. **21**, 51 (1985). A perturbative collision treatment of electronic channel interactions has been developed by A. Giusti, J. Phys. B **13**, 3867 (1980).

[9] H. Rottke and K. Welge, J. Phys. (Paris), Colloq. **46**, C1-127 (1985).

[10] Chris H. Greene, A. R. P. Rau, and U. Fano, Phys. Rev. A **26**, 2441 (1982).

[11] R. G. Parsons and V. F. Weisskopf, Z. Phys. **202**, 492 (1967).

[12] See, e.g., M. Berman, H. Estrada, L. S. Cederbaum, and W. Domcke, Phys. Rev. A **28**, 1363 (1983).

[13] L. Wolniewicz and K. Dressler, J. Chem. Phys. **82**, 3292 (1985).

[14] L. Wolniewicz and K. Dressler, J. Mol. Spectrosc. **77**, 286 (1979).

[15] U. Fano and A. R. P. Rau, *Atomic Collisions and Spectra* (Academic, Orlando, FL, 1986), p. 252.

[16] P. Senn, P. Quadrelli, K. Dressler, and G. Herzberg, J. Chem. Phys. **83**, 962 (1985).

[17] P. Senn and K. Dressler, J. Mol. Struct. **142**, 123 (1986).

[18] P. Quadrelli, L. Wolniewicz, and K. Dressler, private communication.